Available online at www.springerlink.com

Acta Metall. Sin. (Engl. Lett.) Vol.26 No. 6 pp. 761—771 December 2013

ACTA
METALLURGICA SINICA
(ENGLISH LETTERS)

Influence of Spark Plasma Sintering Temperature on the Densification, Microstructure and Mechanical Properties of Al-4.5 wt.%Cu Alloy

S. Devaraj, S. Sankaran† *and R. Kumar*

Department of Metallurgical and Materials Engineering, Indian Institute of Technology Madras (IIT Madras), Chennai 600036, India

[Manuscript received 21 March 2013, in revised form 23 July 2013]

The effect of sintering temperature on the densification mechanisms, microstructural evolution and mechanical properties of spark plasma sintered (SPS) compacts of a gas atomized Al-4.5 wt.%Cu alloy was investigated. The powder particles whose size varied between 10 to 500 μm was subjected to SPS at 400, 450 and 500 °C at a pressure of 30 MPa. The compact sintered at 500 °C exhibited fully dense microstructure which was characterized by a uniform distribution of the secondary phase, free of dendrites and micro-porosity. Microscopy and the SPS data reveal that the events such as particle rearrangement, localized deformation and bulk deformation appear to be the sequence of sintering mechanisms depending on the size range of powder particles used for consolidation. The compact sintered at 500 °C exhibited the highest hardness and compression strength since the microstructure was characterized by fine distribution of precipitates, large fraction of sub-micron grains and complete metallurgical bonding.

KEY WORDS: Spark plasma sintering; Sintering mechanisms; Precipitation; Compression strength

1. Introduction

Al-4.5 wt.%Cu alloys are high strength, light weight, precipitation-hardening structural materials potentially relevant for automotive and aerospace industries[1−5]. The mechanical properties of the alloy produced *via* casting route are generally inferior due to slow cooling rates[6−9]. While, other processing techniques such as spray atomization needs careful optimization of process parameters in order to reduce the porosity and the conventional powder metallurgy route can be very tedious with several processing steps[10,11].

Spark plasma sintering (SPS), on the contrary is one of the promising techniques employed in powder metallurgy route to overcome these difficulties. SPS is a rapid and efficient sintering technique to obtain fully dense material without affecting the grain morphology/specific microstructure of the initial powder particles used for the consolidation[12]. In this process, it is believed that momentarily a strong heat flux is generated between the powder particles by applying high electric current and pulse DC voltage under the recommended pressure. Albeit, limited grain growth has been observed in SPS processed materials in contrast to vacuum hot pressing, the final microstructure of the compact relatively remains unaffected[13]. The electrical field involved in the process, enhances the sintering kinetics and promotes full densification at relatively much lower temperatures in a short time producing invariant microstructures[14,15].

The effect of pulsed current sintering on the microstructure and mechanical properties has been studied in the case of pure and alloyed aluminum powder and the process has promoted fine microstructures with enhanced mechanical properties[16−21]. For

† Corresponding author. Assoc. Prof., Ph.D.; Tel: +91 44 22574776, Fax: +91 44 22574776; E-mail address: ssankaran@iitm.ac.in (S. Sankaran)

DOI: 10.1007/s40195-013-0159-z

instance, the microhardness, fracture toughness and Young′s modulus of Al-Cu-Fe SPS compacts have been found to be superior and the sintered compact is free of pores coupled with high density and limited grain growth[22]. In an another study, Al-Si powder was sintered at a temperature of 450 °C under a pressure of 170 MPa with a holding time of 10 min[23]. The properties of the SPS compacts were compared with a hot extruded material. The results showed that the hot extruded material exhibited superior tensile properties than the SPS processed compact. This was attributed to the healing of residual porosity present in SPS compacts at the peripheral region. It is believed that during SPS process a large direct current and high mechanical pressure promotes the increase in temperature and thus high densification rates in contrast to the constant electric current and higher mechanical pressure[24]. However, the exact mechanism of SPS process is still not established. Several studies reported in the literature were based on the generation of plasma during SPS process. For instance, Tokita reported that the neck formation is due to spark plasma generated during the process[25]. Ishiyama *et al.*[26] showed that the grain size of beryllium sintered by plasma activated sintering was smaller than the grain size sintered by hot pressing. Frei *et al.*[27] reported the enhancement of neck growth under the influence of electromigration. Padmavathi *et al.*[28] showed that the density and mechanical properties of the aluminum alloys significantly improved by increasing the sintering temperature and subsequent aging. However, one of the recent studies reported complete absence of "plasma" during the SPS[29]. Apart from the disagreements in literature on the existence of the plasma during the SPS, there is no concerted acceptance of the sintering mechanisms involved. One of such reported mechanisms during SPS process of alloy powders with narrow particle size range involves the following stages namely; particle rearrangement, localized deformation and gross deformation[30]. However, a comprehensive understanding of the sintering mechanism during SPS is still lacking. In the present study, Al-4.5 wt.%Cu powder with a wide particle size range has been subjected to spark plasma sintering at three different temperatures keeping the applied pressure, holding time and heating rate constant. An attempt is made to arrive at possible mechanisms involved during spark plasma sintering based on the data of punch displacement against the time and the temperature. The effect of sintering temperature on the microstructure evolution and mechanical properties of the SPS compacts is also reported.

2. Experimental

2.1 Particle size distribution and spark plasma sintering

The Microtrac (S3500/3000-WET-0.0215 to 1408 μm) laser particle analyzer (USA) was employed to obtain the size distribution of the atomized powder particles. The powder particles were ultrasonicated for 1 min prior to particle size measurement. The SPS machine, Dr. Sinter 1050 (Japan) was employed to prepare sintered compacts. A graphite die with the dimensions of 30 mm (inner diameter) × 60 mm (height) and two graphite punches with dimensions of 30 mm in diameter and 30 mm height were used for the compaction. The die and punches act as heating elements for the powder particles and are expected to facilitate in spreading the heat uniformly. The sintering was performed under vacuum at three different temperatures of 400, 450 and 500 °C at a heating rate of 50 °C/min, at a pressure of 30 MPa and holding time of 5 min. The temperature of the die was measured with the help of a thermocouple which was inserted into the slot provided on the outer surface of the die. The displacement versus time or temperature of the punches during sintering was measured through the data acquisition system. The sintering time in seconds was calculated from the heating rate of the SPS compacts. The samples sintered at different temperatures are hereafter referred to as S-400, S-450 and S-500 throughout the manuscript.

2.2 Microscopy and X-ray diffraction

The microstructures of powder particles and SPS compacts were characterized employing optical microscopy (Leitz laborex 12 ME, Germany), scanning electron microscopy (FEI Quanta 200, USA) and transmission electron microscopy (Philips CM12, The Netherlands) operating at 120 kV. For metallographic studies, samples of SPS compacts were polished according to standard metallographic procedure and etched with Keller′s reagent. After etching, the samples were rinsed with water and dried in an electric drier. In order to perform TEM analyses, thin slice less than 100 μm was prepared using emery polishing. Small pieces of 3 mm diameter were punched out from the thin foil and they were polished with a twin-jet electropolishing machine using a solution of 10% nitric acid in methanol. The X-ray diffraction studies were carried out using X'Pert PRO PANalytical instrument (The Netherlands) to identify the constituent phases in the powder particles and SPS compacts.

2.3 Physical and mechanical properties

The density of the SPS compacts was measured using a digital balance (CP 124S Sartorius instrument, USA) by Archimides′ principle. The hardness was measured using WOLPERT 402 MVD Vickers microhardness tester (USA). The ageing studies of S-400, S-450 and S-500 were carried at a temperature of 190 °C. The cylindrical compression specimens with dimensions of 5 mm diameter and 10 mm height were machined from the SPS compacts as per ASTM C170/C170M-09 standards. The quasi-static uniaxial

compression tests at room temperature on the sintered samples were conducted using INSTRON 3367 (USA) at an initial strain rate of 0.8×10^{-4} s^{-1}.

3. Results and Discussion

3.1 Microstructural characterization

3.1.1 Powder particles

The size and morphology of the gas atomized powder particles used for the consolidation are shown in Fig. 1(a). The powder particles are produced during the spray atomization process. A wide range in the shape and size of the powder particles are generated after solidification of the droplets during spray atomization by the disintegration of molten metal into a fine spray of different sizes of droplets by transferring the kinetic energy of the gas to the molten metal. The powder particles used for compaction are a conglomeration of spherical, elongated and irregularly shaped particles. Spherical powder particles obviously experience very high cooling rates during the atomization in contrast to elongated and irregular shaped particles. The rapid solidification (high cooling rate) of spherical droplets result in cellular microstructures, while elongated and irregular droplets exhibit dendritic solidification structures (Fig. 1(b) and Fig. 1(c)). The secondary dendritic arm shown in Fig. 1(c) depends on the size of the powder particles and the size increases with increase in the size of the powder particles. The particle distribution plot obtained from laser particle analyser is shown in Fig. 2. The majority of the powder particles are in the size range of 90 to 225 μm, while a small percentage of the particles are found to be in the range of 20 to 50 μm and 400 to 500 μm. The aforementioned microstructural variations are understood in the light of thermal conditions of the droplets arriving at the peripheral region of the substrate. The droplets generated during spray atomization are subjected to high cooling rates in the order of 10^3–10^5 °C/s[31]. The smaller atomized droplets experience extensive undercooling and the extent of the undercooling experienced by the droplets depends on their sizes. The droplets with size approximately between 10 and 25 μm are subjected to heterogeneous nucleation, thereby, increasing the number of nucleation sites leading to cellular growth morphology[32,33]. As the growth rate of the droplets increases, the solidification changes from cellular to dendritic morphology[34–36]. Trivedi *et al.*[37] reported the variation of the microstructures within the droplets of different sizes and observed both dendritic and cellular morphology. Further, they showed that the droplet diameter less than 27 μm exhibited microcellular morphology since the smaller droplets undergo higher undercooling[37]. Hence, the variation in the microstructures observed in different powder particles can be attributed to the nucleation, growth and undercooling of the atomized droplets.

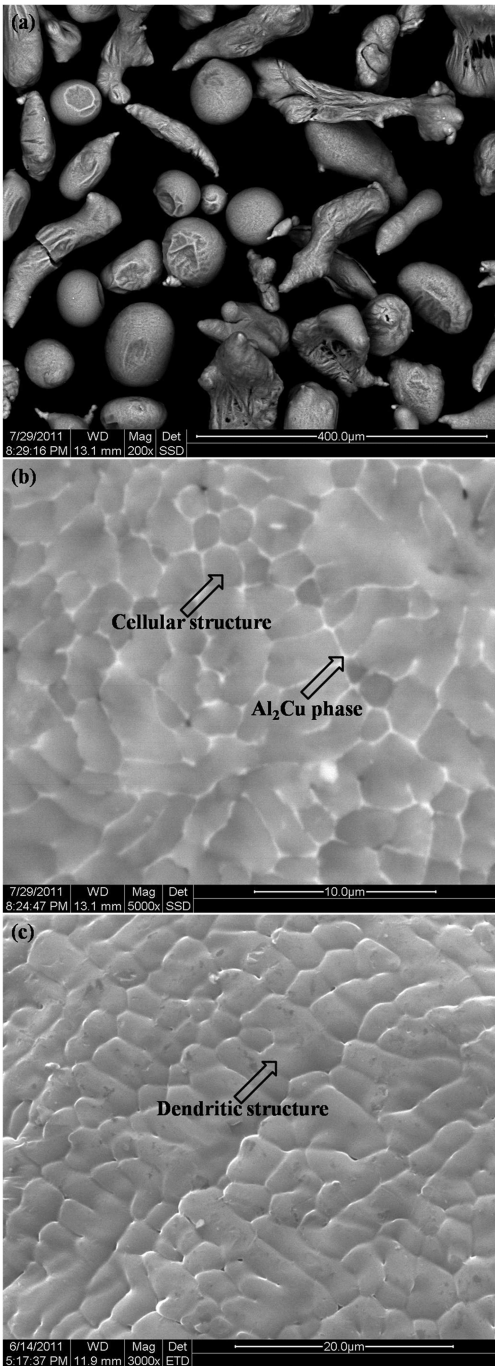

Fig. 1 Scanning electron microscopy micrographs: (a) different sizes and shapes of Al-4.5 wt.%Cu powder particles, (b) spherical powder particle containing cellular morphology, (c) elongated powder particle containing dendritic morphology

3.1.2 Microstructure of SPS compacts

The Al-4.5 wt.%Cu powder was subjected to SPS process and the sintered compacts of size 30 mm in diameter and approximately 10 mm in height were produced. The relative densities of the SPS compacts, S-400, S-450 and S-500 are 95%, 98% and 99%, respectively. There is an obvious increase in the density of the compacts with increase in sintering tem-

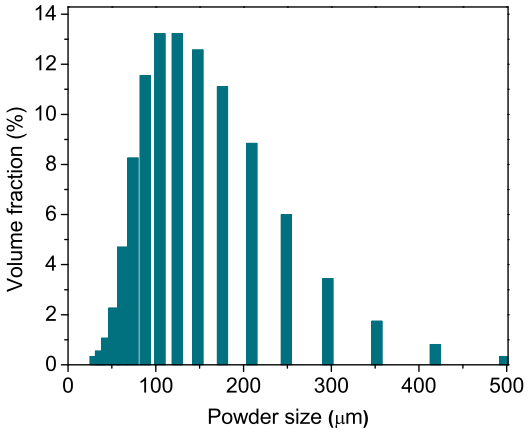

Fig. 2 The powder particle size distribution as obtained from laser particle analyser

perature. The light micrographs of S-400, S-450 and S-500 exhibiting microstructural variations within the compacts are shown in Fig. 3. While some regions of the SPS compacts show cellular morphology, the other regions exhibit dendritic morphology (Fig. 3(a) and Fig. 3(b)). The compacts retain the same morphology as that of the powder particles even after sintering. This suggests that during SPS process local melting takes place only at the surface of the individual particles which come in contact and the metallurgical bonding occurs[22]. It appears that the sintering temperature and pressure do not affect the morphology of the powder completely because of very short time scales during sintering. Fig. 3(c) indicates that the microstructure of the compact sintered at 500 °C is free from the dendritic structures. At a temperature of 500 °C the dendritic arms are disintegrated into a number of individual particles and they no longer are interconnected. In contrast, the compacts sintered at the temperatures of 400 and 450 °C retain the dendritic structures due to insufficient driving force for the disintegration. The observed microstructural variations within the same compact strongly depend on the size of the powder particles used for compaction. It may be noted that the compacts S-400 and S-450 almost retain the similar microstructural features as observed in the powder particles with small fraction of partially deformed particles, whereas, in the case of compact sintered at 500 °C (S-500) the secondary phase is completely dispersed in the matrix.

The XRD shown in Fig. 4(a) and Fig. 4(b) confirm the presence of Al and Al_2Cu phases in powder particles as well as in the SPS compacts. The absence of oxide peaks in the diffractogram indicates that the atomization in nitrogen atmosphere protected the droplets from oxidation.

The SEM micrographs of SPS compacts reveal the distribution of second phase along the grain boundaries in concomitant to interparticle boundaries as observed in Fig. 5. However, the compact sintered at 500 °C confirms the second phase particles not only

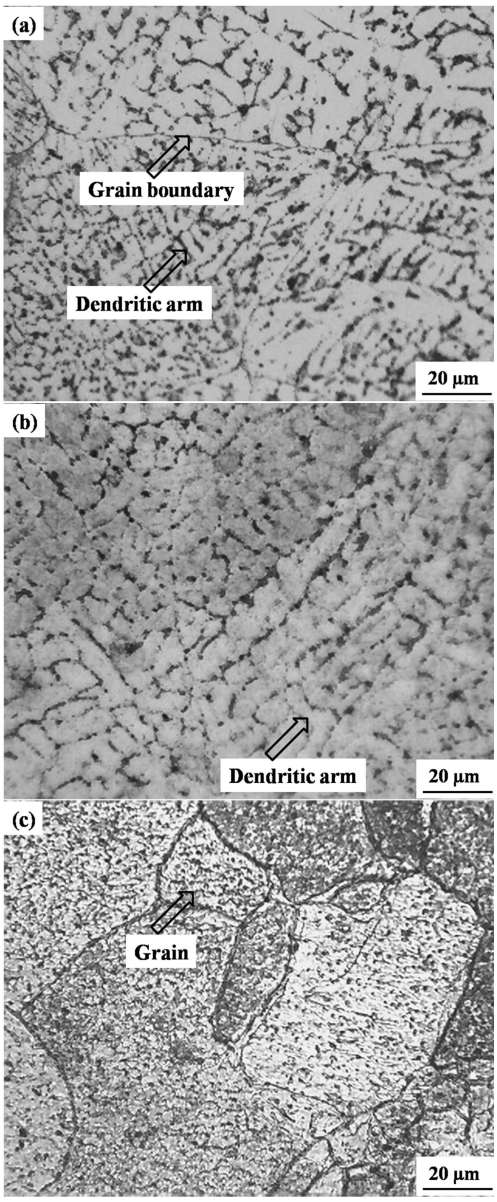

Fig. 3 Optical micrographs of SPS compacts: (a) and (b) sintered at 400 and 450 °C containing dendritic structure, (c) sintered at 500 °C containing the disintegrated Al_2Cu phase

exists along the boundaries but also well dispersed in the interior of the grains (Fig. 5(c)). This is possibly due to sintering at that particular temperature promoting dissolution of the metastable precipitates and transforming remaining copper from the solid solution to equilibrium phases. However, a detailed study is necessary to understand the effect of SPS process parameters on the precipitation behavior. Fig. 5d shows a high magnification SEM image of the distribution of the second phases along the grain boundaries and the inserts are the energy dispersive X-ray spectroscopy (EDS) results obtained from the second phase distributed along the grain boundaries and the matrix. The bright field TEM micrographs of SPS compact processed at 500 °C are presented in Fig. 6(a). It can

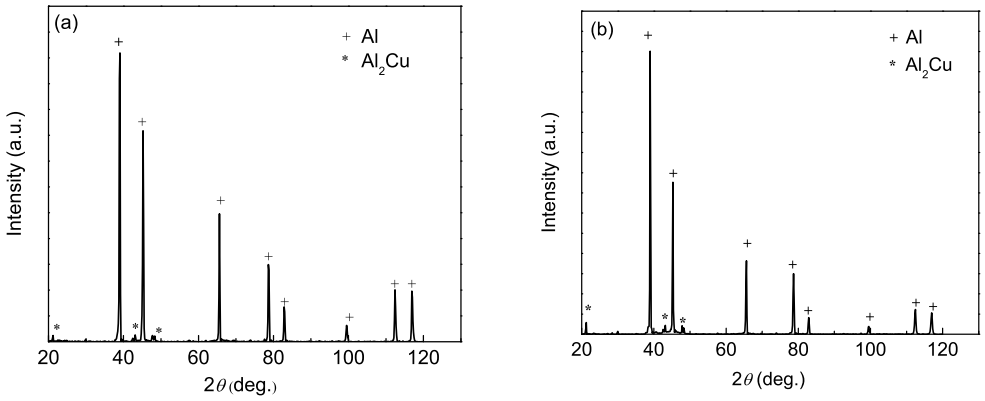

Fig. 4 X-ray diffractograms of Al-4.5 wt.%Cu powder (a) and SPS compacts confirming the presence of Al_2Cu phase in Al matrix (b)

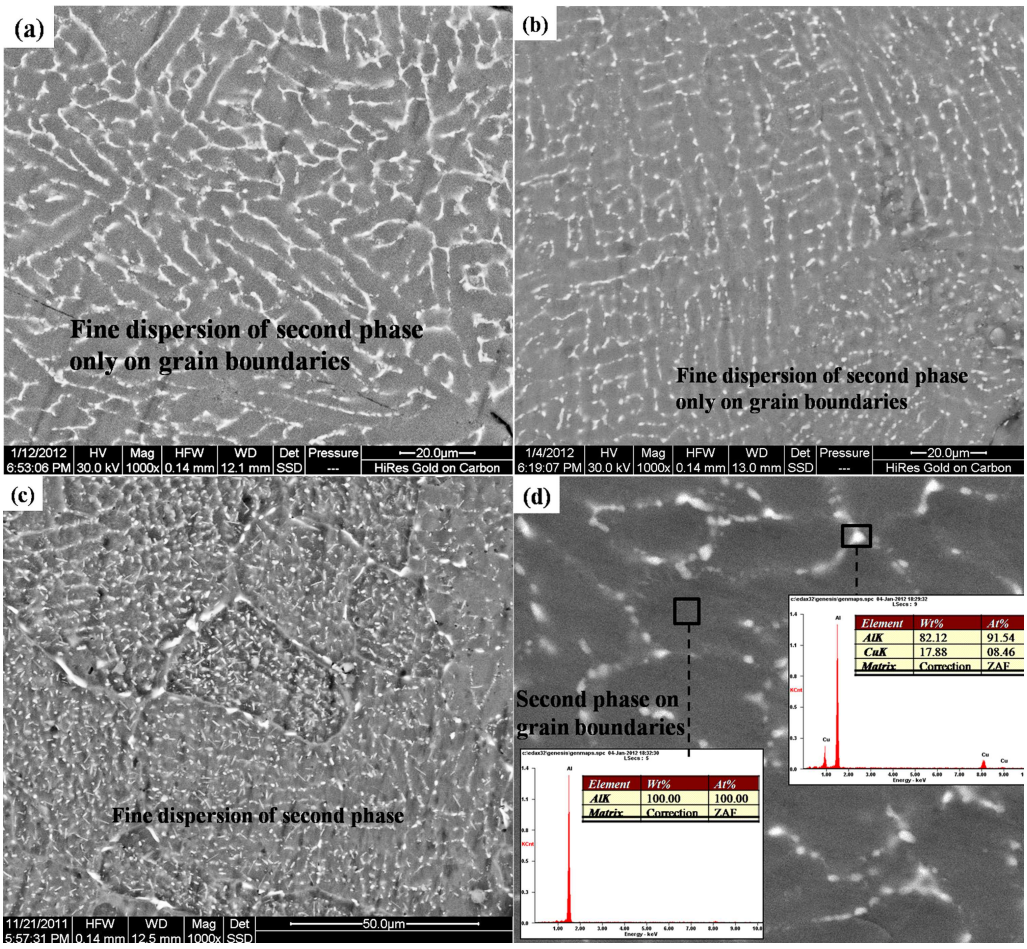

Fig. 5 Scanning electron micrographs of the sintered compacts exhibiting dispersion of the second phase particles as the function of sintering temperatures 400, 450 and 500 °C: (a, b) primarily on the grain boundaries, (c) on grain boundaries as well as in the interior of the grains, (d) high magnification image exhibiting the distribution of second phase particles on the grain boundaries, and the insert shows the EDS analysis confirming the copper rich particles appear primarily on the grain boundaries as compared to the grain interior

be noted that the microstructure is typical and appears to consist of coarse grains surrounded by very fine recrystallized sub-micron grains (100–300 nm). This is possibly due to two primary reasons: (a) large particle size difference in the powder particles and (b) local melting around the particles in very short duration, would have promoted localized recrystalization of fine grains around the coarse particles. However, majority of the microstructure is characterized by the coarse grained structure with uniform dispersion of

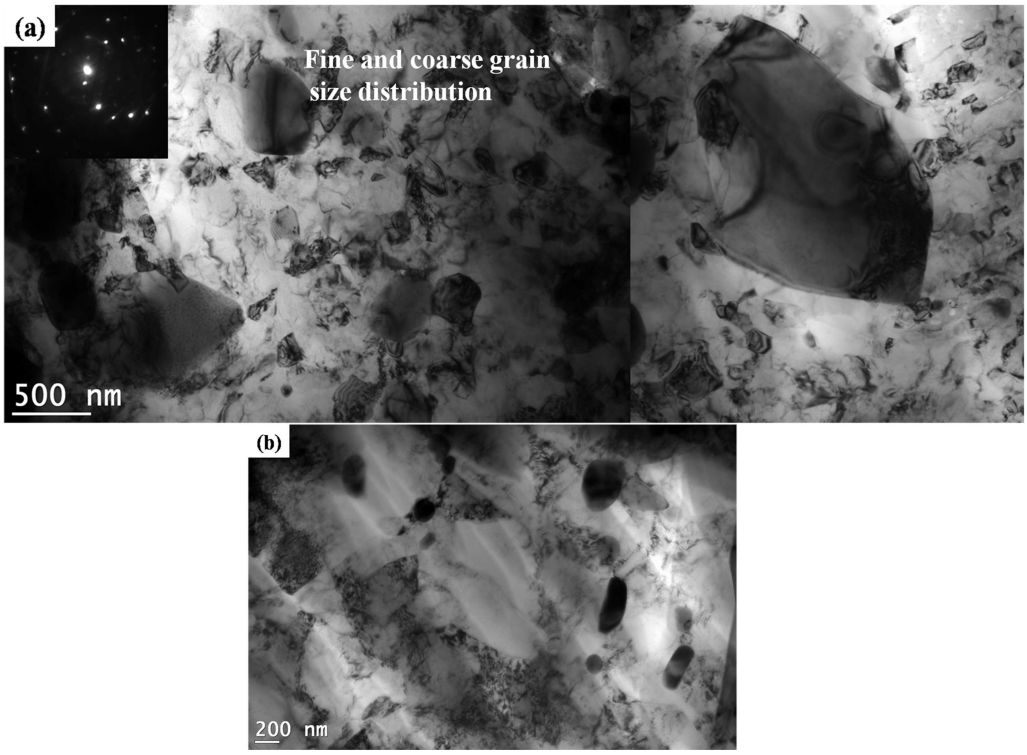

Fig. 6 Bright field TEM images of S-500: (a) presence of the sub grains and insert showing the corresponding diffraction pattern, (b) the sub-grains with Al_2Cu precipitates

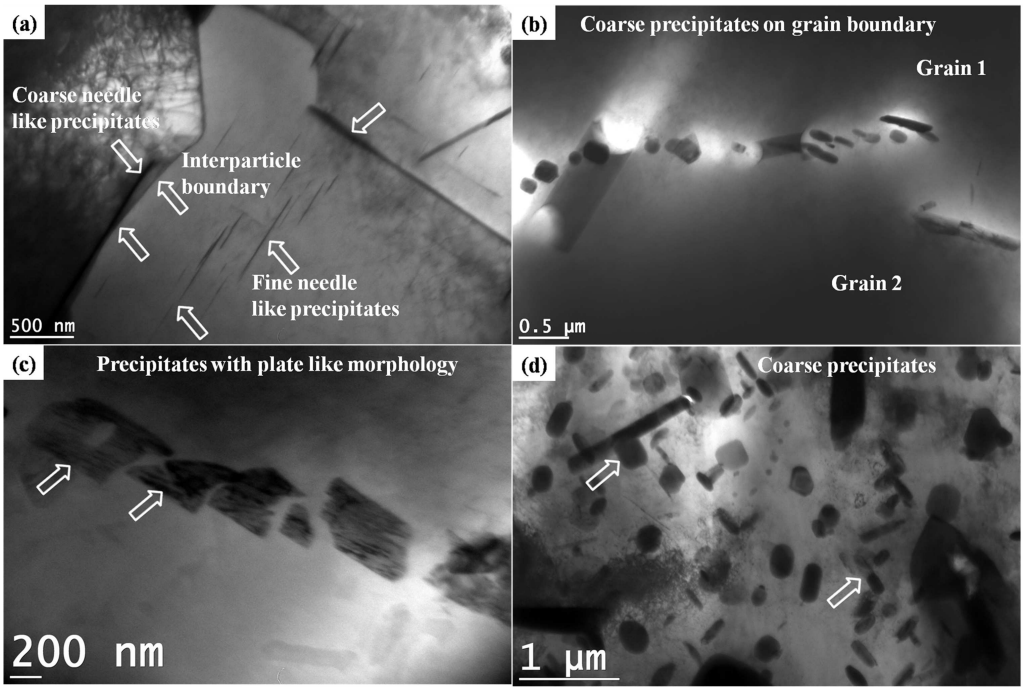

Fig. 7 Bright field TEM micrographs of the compact (500 °C) showing the presence of Al_2Cu precipitate phase: (a) coarse and fine needle like precipitates within the grain and the grain boundaries, (b) coarse precipitates on the grain boundary, (c) plate like precipitates, (d) different kind of the coarse precipitates

Al_2Cu precipitates as shown in Fig. 6(b). The bright field TEM micrographs of the precipitates of different morphology present in the SPS compact sintered at 500 °C are exemplified in Fig. 7(a)–Fig. 7(d). In general, three types of morphologies are identified namely needle-like precipitates (Fig. 7(a)), coarse irregular precipitates along the grain boundary and in matrix (Fig. 7(b) and Fig. 7(d)), and irregular plate-like

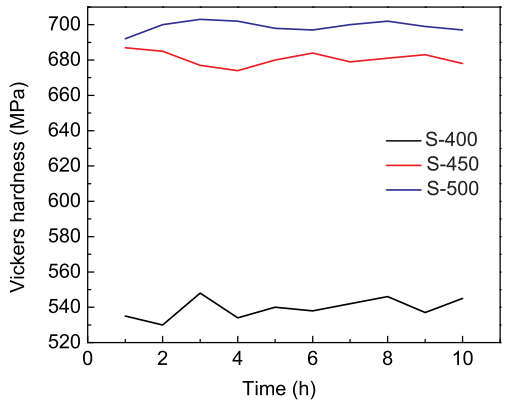

Fig. 8 Ageing curves showing the variation in hardness for different SPS compacts

(Fig. 7(c)) precipitates. In general, the equilibrium Al_2Cu precipitates (θ phase) are coarse and they are a few microns and sub-micron in size. In Al-Cu system, the other intermediate metastable phases such as θ" or θ' have needle morphology. It is believed that since during the atomization process each droplets undergo different rates of the undercooling, each solidified particle is expected to contain mixture of these intermediate metastable phases. However, these intermediate precipitates are present in very small fraction as compared to the coarse stable phase; they do not contribute to the precipitation strengthening of the alloy. This is confirmed through the results of ageing studies of the alloy at different time duration presented in Fig. 8. There is no significant variation in hardness in SPS compacts even after 10 hours of heat-treatment. Hence, it is clear from the plot that there is no contribution from the small fraction of intermediate precipitates.

3.1.3 Densification mechanisms during sintering

The mechanism of sintering during the SPS process when the powder particles with a wide range of particle size distribution used for consolidation is of considerable interest. During the SPS process, the powder particles were subjected to compression between top and bottom punches and the die wall. It is possible to obtain the displacement or displacement rate data of punch as a function of time or temperature during sintering. The typical displacement and displacement rate versus temperature plots obtained during sintering of the three compacts are presented in Fig. 9(a)—Fig. 9(c)). The characteristic plot obtained for each compact pertaining to particular sintering temperature can be related to the mechanisms of densification of the powder particles. Such analysis was reported in literature for identifying the densification mechanisms of the powder particles during SPS process[30]. It can be seen from Fig. 9 that the maximum displacement of the powder particles that takes place is 10 mm (Fig. 9(a)) at 400 °C. When the sintering temperature is increased to 450

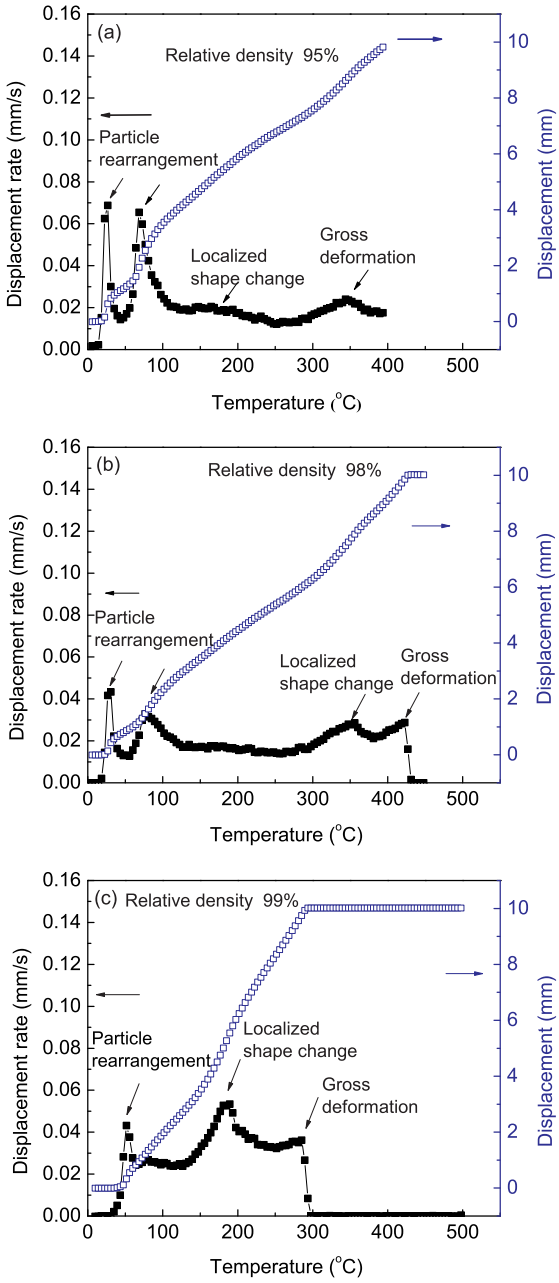

Fig. 9 Displacement rate and displacement *vs.* temperature plots for S-400 (a), S-450 (b) and S-500 (c)

or 500 °C, the displacement remains constant (Fig. 9(b) and Fig. 9(c)). However, the displacement rate exhibits multiple peaks at intermediate temperatures before complete sintering occurs. In general, there are 3 to 4 displacement peaks observed for the three sintering temperatures employed. The micrographs of S-400 and S-450 show a porosity of ~6 vol.% and ~ 2 vol.%, respectively, indicating that the powder particles are not sintered well to each other at the contact points (Fig. 10(a) and Fig. 10(b)). This could possibly be attributed to insufficient heat available for S-400 and S-450 for complete metallurgical bonding to occur between the powder particles and remove solid-vapor interfaces. On the contrary, microstructural features of

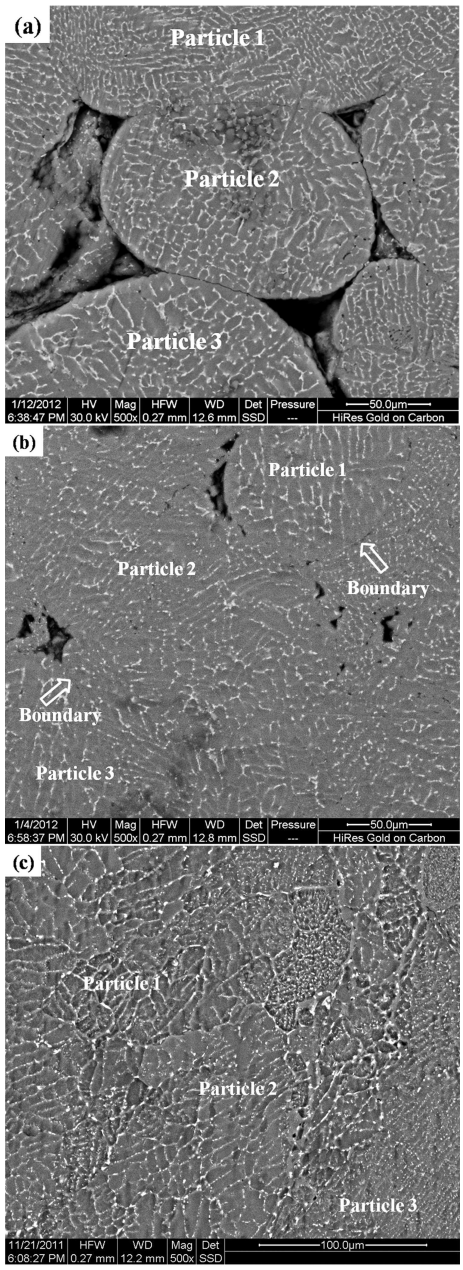

Fig. 10 SEM micrographs of S-400 (a), S-450 (b) and S-500 (c) exhibiting the degree of metallurgical bonding between the particles as a function of processing temperatures

S-500 indicate no porosity and excellent metallurgical bonding between the powder particles (Fig. 10(c)). Due to low voltage and high pulsed current, the sparks produced between the powder particles might create high temperatures within a short period of time. As a consequence, necks are formed between the powder particles and this leads to volume diffusion through the contact points of the powder particles[25]. The localized heat transfer spread uniformly across the sample resulting in the elimination of the porosity. It is clear from the micrographs and density measurements that during sintering, the densification is not completely achieved below 500 °C. In addition to the above observation, the three stage mechanism (particle rearrangement, local deformation and bulk deformation) proposed apriori[30] is corroborated by the micrographs presented in the Fig. 8 and Fig. 10(a), 10(b) and 10(c) and also shown as schematic in the Fig. 11 and Fig. 12. In the first case (Fig. 11) the compact contains a wide range of particle sizes and the second case (Fig. 12) the compact contains a narrow range of particle sizes. The two peaks appear below 100 °C in Fig. 9(a) and Fig. 9(b) possibly related to the particle rearrangement especially the compact containing particles with size range around 400–500 μm to 20–50 μm. The initial rearrangement of the coarse particles occurs followed by the flow of fine particles into the voids that are generated in between the coarse particles (Fig. 11). These two events are expected to cause displacement rate peak at the initial stages of sintering. However, the second peak of displacement rate is not expected to appear if the compact contains only narrow range of particle sizes. Subsequently, the second and third peaks correspond to the local shape change and bulk deformation of the compact respectively.

The sizes of the powder particles also play a significant role in sintering mechanisms[30]. The rearrangement of the particles is done by application of pressure through the relative motion between the powder particles. The contact points between the powder particles per unit volume are decreased by increasing the particle size and hence rearrangement of the particles is enhanced. On the other hand, if the particle size is decreased the peak height is decreased thereby increasing the local deformation. For instance, the maximum displacement observed in Fig. 9 could be primarily attributed to the sizes of the powder particles used as exemplified in Fig. 11 and Fig. 12. The consolidation/displacement occurs in different stages depending on the size of the powder particles. Fig. 11 exemplifies the displacement when a wide size range of the powder particles are used occurring in two stages. During the initial stage of sintering, the coarse particles are rearranged followed by the rearrangement of fine particles during the next stage which obviously are a function of the temperature and time. On the contrary, the displacement of the uniform sized powder particles are arranged in a single stage as shown in Fig. 12. The displacement when the uniform sized powder particles are used occurs much earlier to establish the contact between the powder particles compared to the case when the distribution is large. This could be possibly the reason that the displacement reached maximum below 300 °C when the powder was sintered at 500 °C in contrast to compacts sintered at 400 and 450 °C.

3.2 Hardness and compression properties

The average hardness values of S-400, S-450 and S-500 are (539±38), (687±24) and (703±27) MPa, respectively. The hardness of S-500 is 23% higher than

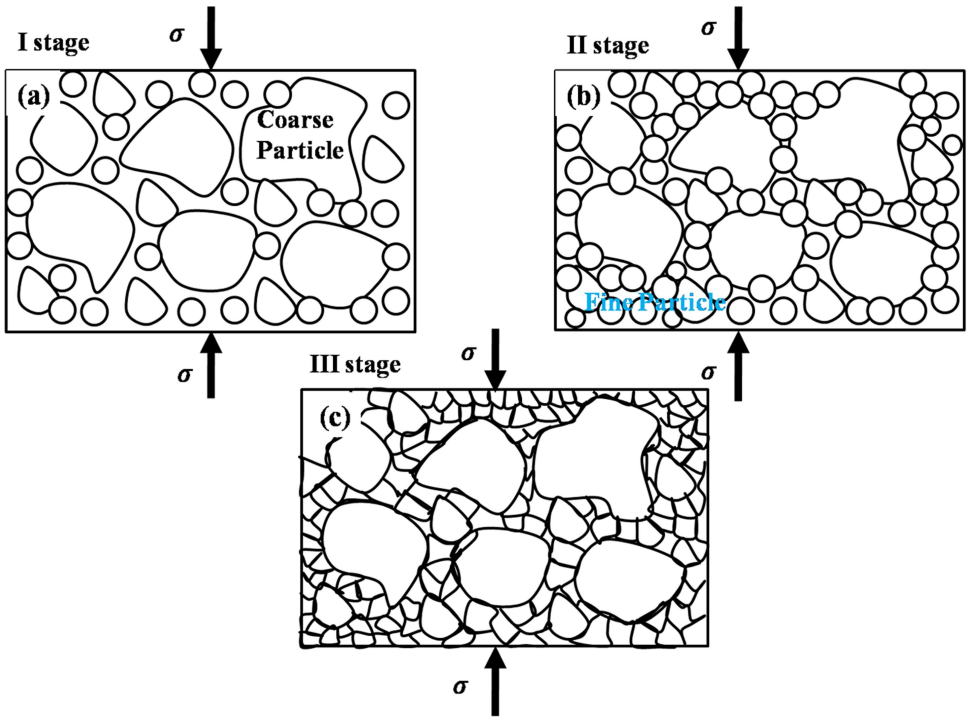

Fig. 11 Schematic representation of consolidation of the powder with wide range of particle size: (a) consolidation of the coarse particle at first stage with particle rearrangement, (b) consolidation of fine particles at second stage with local deformation, (c) the grains after sintering with bulk deformation

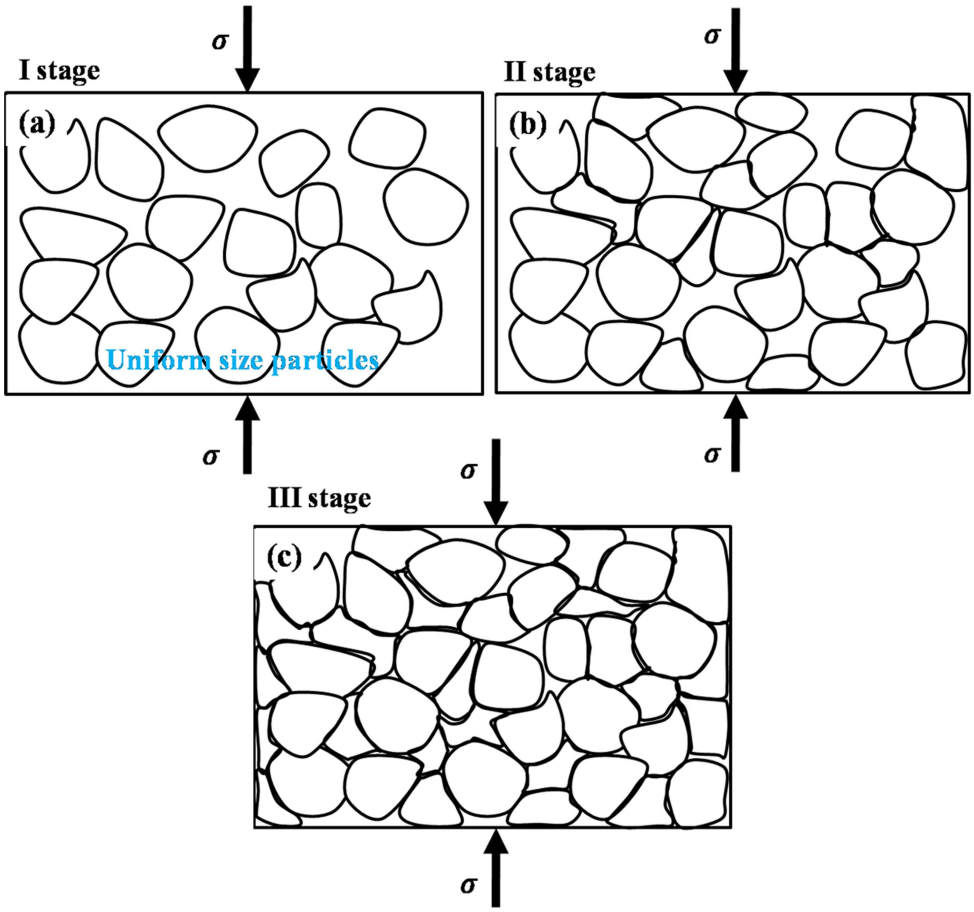

Fig. 12 Schematic illustrates the consolidation of the powder with narrow range of particle size: (a) consolidation of coarse particle at first stage with particle rearrangement, (b) consolidation of the fine particles at second stage with local deformation, (c) the grains after sintering with bulk deformation

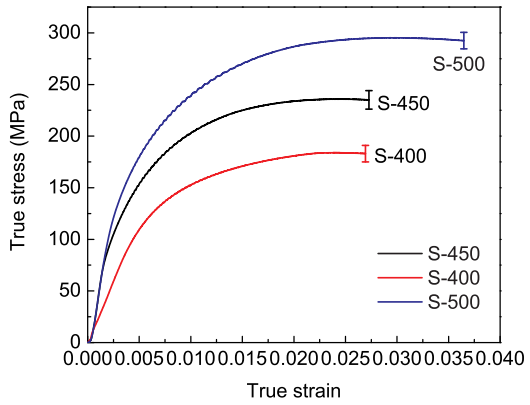

Fig. 13 True stress *vs.* true strain curves of SPS compacts sintered at different temperatures

that of S-400. Understandably, the low hardness value reported for S-400 is primarily attributed to incomplete densification and poor metallurgical bonding. The increase in hardness of S-500 can also be attributed to the presence of the sub-micron grains as noticed in Fig. 6(a) and Fig. 6(b). The true stress and true strain plots of the SPS compacts are shown in Fig. 13 after compliance correction. The quasi-static compression strengths of S-400, S-450 and S-500 compacts are found to be (182±8), (238±9) and (290±8) MPa respectively. All the samples flattened upon compression and did not rupture indicating retention of the ductility. The reason for the increased compression strength of S-500 is primarily attributed to the presence of sub-micron grains (Fig. 6(a) and Fig. 6(b)) with precipitates, also Al_2Cu precipitates along the grain boundaries as well as within the grains as observed in TEM micrographs (Fig. 6(a)—Fig. 6(d)) concomitant to strong metallurgical bonding. Also, it is expected that the precipitates act as the barriers to the grain boundary movement and to the motion of the dislocations.

4. Conclusions

(1) The atomized powder comprises of spherical, elongated and irregular shape of the powder particles. The spherical powder particles exhibited cellular morphology, whereas the elongated and the irregular shape of the particles revealed the dendritic structure due to differences in the cooling rates of droplets.

(2) The sintering temperature has a profound influence on the densification, microstructure and mechanical properties. The spark plasma sintering carried out at 500 °C revealed more dense and uniform distribution of the secondary phase free of the dendrites in contrast to those carried out at 400 and 450 °C.

(3) The microscopy and the SPS data revealed that the particle rearrangement, localized deformation and bulk deformation appears to depend on the size of the powder particles used for consolidation.

(4) The compact sintered at 500 °C exhibited the highest hardness and highest compression strength since the microstructure was characterized by fine distribution of the precipitates, large fraction of sub-micron grains and complete metallurgical bonding.

Acknowledgements

The authors would like to express sincere thanks to Mr. Sujith. R, Mr. Niraj Chawake and Mr. Bobu Manuel Jolly for their technical support during the SPS process. Also, sincere thanks are extended to Mr. N. Raghukiran, Mrs. D. Kanchanamala and Mr. S. Veerabathiran for helping in the TEM laboratory.

REFERENCES

[1] J.M. Silcock, T.J. Heal and H.K. Hardy, J. Inst. Met. **82** (1954) 239.
[2] A. Guinier, Solid State Phys. **9** (1959) 293.
[3] U.H. Gläser, G. Dlubek and R. Krause, Phys. Status. Solidi B. **163** (1991) 337.
[4] Y. Nagai, M. Murayama, Z. Tang, T. Nonaka, K. Hono and M. Hasegava, Acta. Mater. **49** (2001) 913.
[5] S.C. Wang and M.J. Starink, Int. Mater. Rev. **50** (2005) 193.
[6] H.D. Brody and M.C. Flemings, Trans. Met. Soc, AIME. **236** (1966) 615.
[7] T.Z. Kattamis, J.C. Coughlin and M.C. Flemings, Trans. Met. Soc. AIME. **236** (1967) 1504.
[8] T.Z. Kattamis, Y.V. Mirty and J.A. Reffner, J. Crystal Growth. **19** (1973) 237.
[9] G. Baumeister, B. Okolo and J. R?gner, Microsyst. Technol. **14** (2008) 1647.
[10] A.R.E. Singer, Met. Mater. **4** (1970) 246.
[11] S.M. Lee, J.H Jung, E. Fleury, W.T. Kim and D.H. Kim, Mater. Sci. Eng. A. **294-296** (2000) 99.
[12] M. Tokita, J. Soc. Powder Technol. Jpn. **30** (1993) 790.
[13] J.K. Rana, Development of Bulk Nanocrystalline High Strength AA6061 Aluminum Alloy by High Energy Ball Milling, M. Technol Thesis, Indian Institute of Technology Madras, 2008.
[14] J.R. Groza and A. Zavaliangos, Mater. Sci. Eng. A. **287** (2000) 171.
[15] R. Chaim, Mater. Sci. Eng. A. **443** (2007) 25.
[16] J.R. Ryu, K.I. Moon and K.S. Lee, J. Alloys Compd. **296** (2000) 157.
[17] Y. Murakoshi, T. Sano, I. Diewwanit, Y. Nakayama and S. Miyamoto, Proceedings of the 1st International Symposium on Spark Plasma Sintering (ISSPS-1), Singapore, September 06-08, 2001.
[18] O. Ohashi, G. Xie and K. Chiba, Spark Plasma Sintering of Pure Aluminum Powder and Bonding Behavior Powder Particles. Proceedings of the 1st International Symposium on Spark Plasma Sintering (ISSPS-1), Singapore, September 06-08, 2001.
[19] Y. Shiomi, J. Yoshino and N. Kuroishi, SPS Sintered Pre-Forms for High Strain Rate Super Plastic Forming. Proceedings of the 1st International Symposium on Spark Plasma Sintering (ISSPS-1), Singapore, September 06-08, 2001.

[20] G. Xie, O. Ohashi and N. Yamaguchi, Trans. Mater. Res. Soc. Jpn. **27** (2002) 743.
[21] T. Nagae, M. Yokota, M. Nose, S. Tomida, K. Otera, T. Kamiya and S. Saji, Mater. Trans. **43** (2002) 537.
[22] E. Fleury, J.H. Lee, S. H. Kim, G.S. Song, J.S. Kim, W.T. Kim and D.H. Kim, Mater. Res. Soc. Symp. **643** (2001) K2-1-1.
[23] Th. Schubert, J. Schmidt, T. Weissgärber and B. Kieback, World Powder Metallurgy Congress and Exhibition, PM-2010, Florence, Italy, October 10-14, 2010.
[24] S.W. Wang, L.D. Chen, Y.S. Kang, M. Niino and T. Hirai, Mater. Res. Bull. **35** (2000) 619.
[25] M. Tokita, J. Soc. Powder. Technol. Jpn. (1993) 790.
[26] M. Ishiyama, Y. Bando and K. Kosuge, Proceedings of 1993 Powder Metallurgy World Congress, Japan Society of Powder and Powder metallurgy, Japan, 1993, p.931.
[27] J.M. Frei, U.A. Tamburini and Z.A. Munir, J. Appl. Phys. **101** (2007) 114914.
[28] C. Padmavathi, A. Upadhyaya and D. Agarawal, Mater. Chem. Phys. **130** (2011) 440.
[29] D.M. Albert, A. Anders, D.V. Dudina, J. Andersson, D. Jiang, C. Unuvar, U.A. Tamburini, E.J. Lavernia and A.K. Mukherjee, J. Appl. Phys. **104** (2008) 033305.
[30] S. Diouf and A. Molinari, Powder Technol. **221** (2012) 220.
[31] R. Mehrabian, Int. Met. Rev. **27** (1982) 185.
[32] R. Willnecker, D.M. Herlach and B. Feuerbacher, Appl. Phys. Lett. **49** (1986) 1339.
[33] J.H. Perepezko, Mater. Sci. Eng. **65** (1984) 125.
[34] A.K. Srivastava, S.N. Ojha and S. Ranganathan, Metall. Mater. Trans. A **29** (1998) 2205.
[35] M. Gupta, F. Mohamed and E.J. Lavernia, Metall. Trans. A **23** (1992) 831.
[36] Y. Abe, K. Miyasawa and M. Nakamura, Mater. Sci. Eng. **98** (1998) 351.
[37] R. Trivedi, F. Jin and I.E. Anderson, Acta Mater. **51** (2003) 289.